which is valid between the two walls. Figure 6.1 presents the wave function, the probability density, and the energy spectrum. The lowest-lying state at E_1, called the *ground state*, has a finite energy $E_1 > 0$, which implies a kinetic energy $E_{\text{kin}} > 0$ since the potential energy V is zero by construction. Already this situation differs from that in classical mechanics, where the state of least energy is of course the state of rest with $E = E_{\text{kin}} = 0$. The higher states increase in energy proportionally to n^2. The *quantum number* n is equal to one plus the number of nodes of the wave function in the region $-d/2 < x < d/2$; that is, the boundaries $x = \pm d/2$ are excluded. The wave function has even or odd symmetry with respect to the point $x = 0$, depending on whether n is odd or even, respectively. Even wave functions, here the cosine functions, are said to possess *even* or *natural parity*, odd wave functions *odd* or *unnatural parity*. Obviously, wave functions with an even number of nodes have even parity, those with an odd number odd parity. This property also holds for other one-dimensional potentials that are mirror-symmetric.

6.2 Particle Motion in a Deep Square Well

In Section 6.1 we found the spectrum of eigenvalues E_n and the wave functions describing the corresponding eigenstates $\varphi_n(x)$ for the deep square well. The solutions of the time-dependent Schrödinger equation are obtained by multiplying $\varphi_n(x)$ with a factor $\exp(-\mathrm{i}E_n t/\hbar)$. Through a suitable superposition of such time-dependent solutions, we form a moving wave packet which at the initial time $t = 0$ is bell shaped with a momentum average p_0. Its wave function is

$$\psi(x,t) = \sum_{n=1}^{\infty} a_n(p_0, x_0)\varphi_n(x) \exp\left[-\frac{\mathrm{i}}{\hbar}E_n t\right] \quad ,$$

where the coefficients $a_n(p_0, x_0)$ have been chosen to ensure a bell shape around location x_0 for $t = 0$ and the momentum average p_0.

Figure 6.2 shows the time development of the probability density $|\psi(x,t)|^2$ for such a wave packet. We observe that for $t = 0$ the wave packet is well localized about initial position x_0 of the classical particle. It moves toward one wall of the well, where it is reflected. Here it shows the pattern typical of interference between incident and reflected waves. The pattern is very similar to that caused by a free wave packet incident on a sharp potential step, shown in Figure 5.2c. It continues to bounce between the two walls and is soon so wide that the packet touches both walls simultaneously, showing interference patterns at both walls.

It is interesting to see how the spatial probability density $\rho^{\text{cl}}(x,t)$ derived from a classical phase-space probability density behaves in time. This is

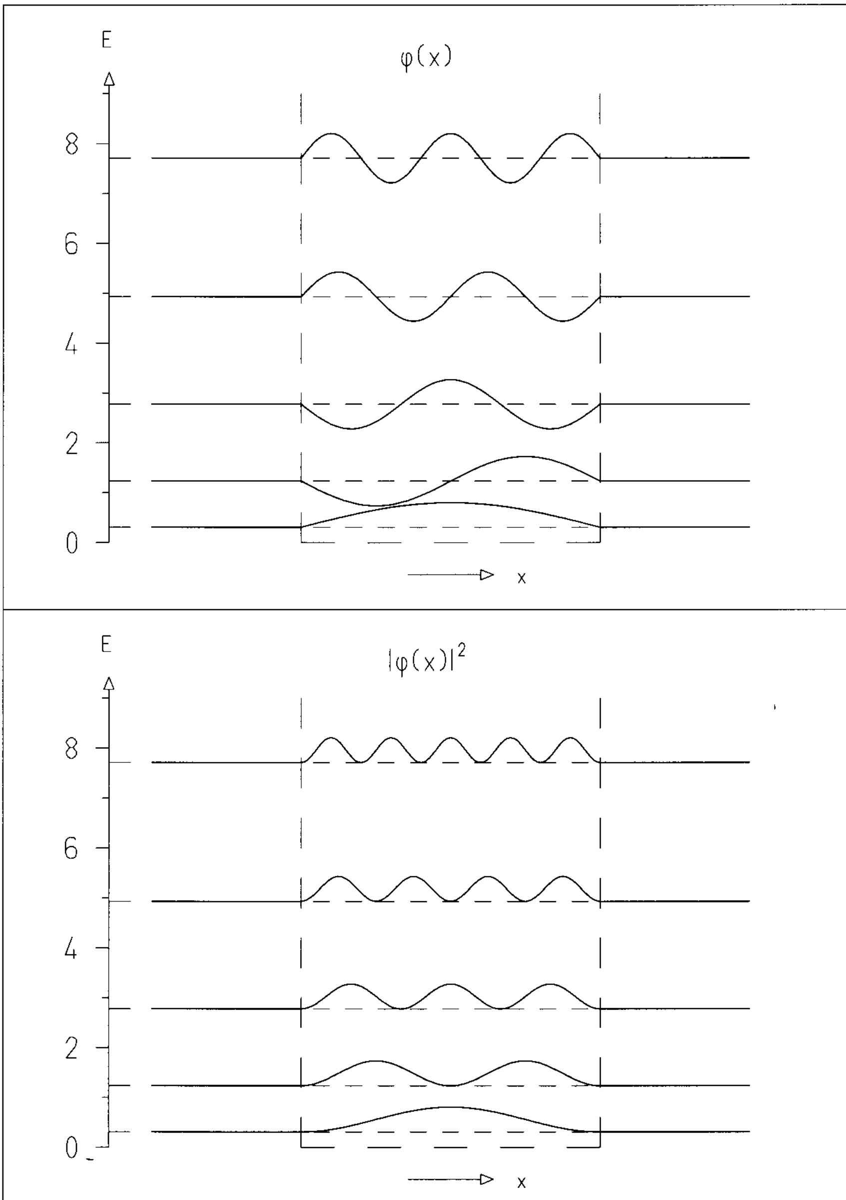

Fig. 6.1. Bound states in an infinitely deep square well. The long-dash line indicates the potential energy $V(x)$. It vanishes for $-d/2 < x < d/2$ and is infinite elsewhere. Points $x = \pm d/2$ are indicated as vertical walls. On the left side an energy scale is drawn, and to the right of it the energies E_n of the lower-lying bound states are indicated by horizontal lines. These lines are repeated as short-dash lines on the left. They serve as zero lines for the wave functions $\varphi(x)$ and the probability densities $|\varphi(x)|^2$ of the bound states.

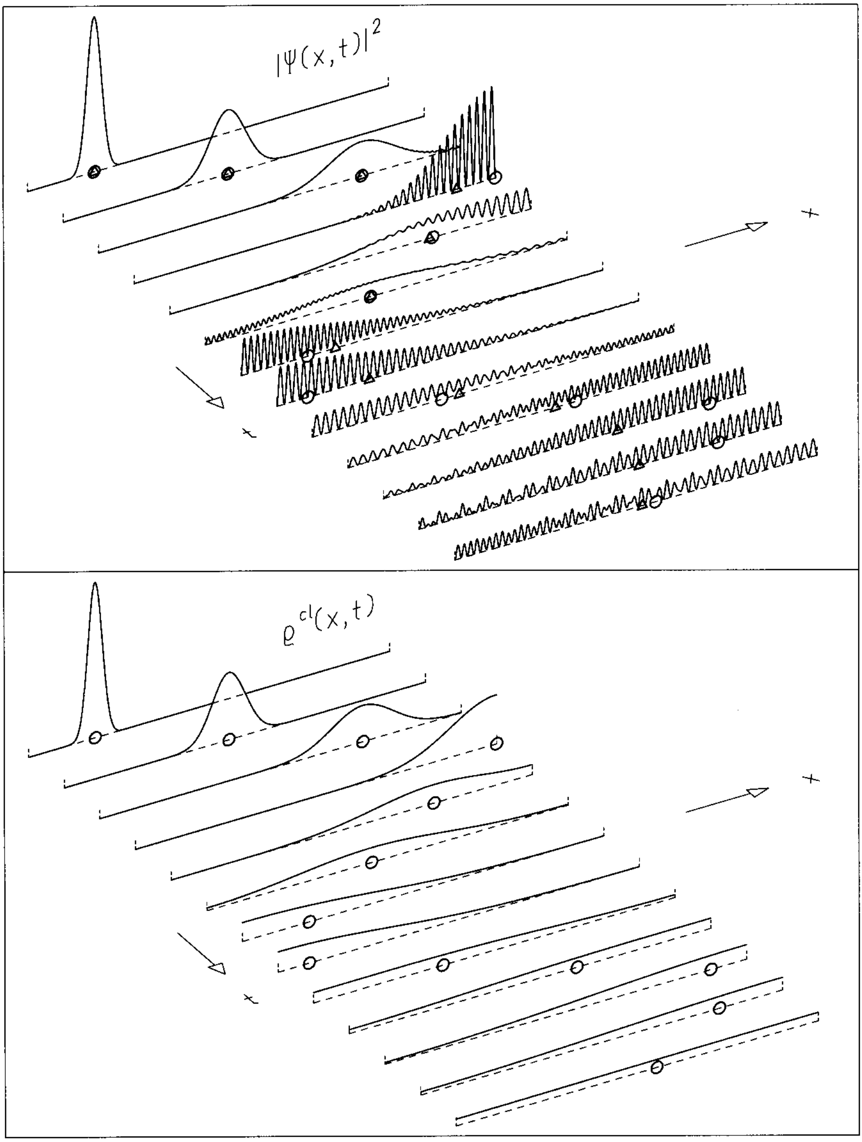

Fig. 6.2. Top: Time development of a wave packet moving in an infinitely deep square well. At $t = 0$, in the background, the smooth packet is well concentrated. Its initial momentum makes it bounce back and forth between the two walls. The characteristic interference pattern of the reflection process, as well as the dispersion of the packet with time, is apparent. The small circle indicates the position of the corresponding classical particle. The quantum-mechanical position expectation value is shown by a small triangle. Bottom: Time development of the spatial probability density computed from the classical phase-space distribution corresponding to the quantum-mechanical wave packet.

shown in the bottom part of Figure 6.2. As long as the bulk of the probability density is not close to the walls the quantum-mechanical density $|\psi(x,t)|^2$ and the classical density $\rho^{\mathrm{cl}}(x,t)$ are very similar.

Near the walls, however, the quantum-mechanical wave packet displays the interference pattern typical for the superposition of the two wave functions incident on and reflected by the wall. As the packet disperses the interference pattern fills the whole well. No interference is observed in the time development of the classical phase-space density. It is obtained as the sum

$$\begin{aligned}\rho_x^{\mathrm{cl}}(x,t) &= \frac{1}{\sqrt{2\pi}\sigma_x(t)}\sum_{n=-\infty}^{\infty}\left\{\exp\left[-\frac{(x-v_0t-2nd)^2}{2\sigma_x^2(t)}\right]\right.\\ &\left.+\exp\left[-\frac{(x+v_0t-(2n+1)d)^2}{2\sigma_x^2(t)}\right]\right\}\end{aligned}$$

with the time-dependent width of a free wave packet:

$$\sigma_x(t) = \sigma_{x0}\sqrt{1+\left(\frac{\sigma_p t}{\sigma_{x0}m}\right)^2}$$

by a simple generalization of the sum at the end of Section 5.2 from the reflection at one high potential wall to the repeated reflection between two high walls.

We now want to study the quantum-mechanical wave packet in a deep well over a much longer period of time. At the end of the time interval studied in Figure 6.2 the quantum-mechanical probability density $|\psi(x,t)|^2$ occupies the full width of the well and one might be inclined to think that it continues to do so. It is easy to see, however, that the quantum-mechanical wave function $\psi(x,t)$ must be periodic in time, the period being

$$T_1 = \frac{2\pi}{\omega_1} \quad ,$$

where ω_1 is the frequency of the ground-state wave function

$$\omega_1 = \frac{E_1}{\hbar} = \frac{\hbar}{2m}\left(\frac{\pi}{d}\right)^2 \quad .$$

Since all energies E_n, $n = 2, 3, \ldots$, are integer multiples of E_1, the period T_1 of the ground state is also the period of the superposition $\psi(x,t)$ that describes the wave packet. Because of this periodicity in time the original wave packet must be restored after the time T_1 has elapsed. In Figure 6.3 we show the time dependence of the same wave packet as in Figure 6.2 over a full period T_1 and find our expectation verified.

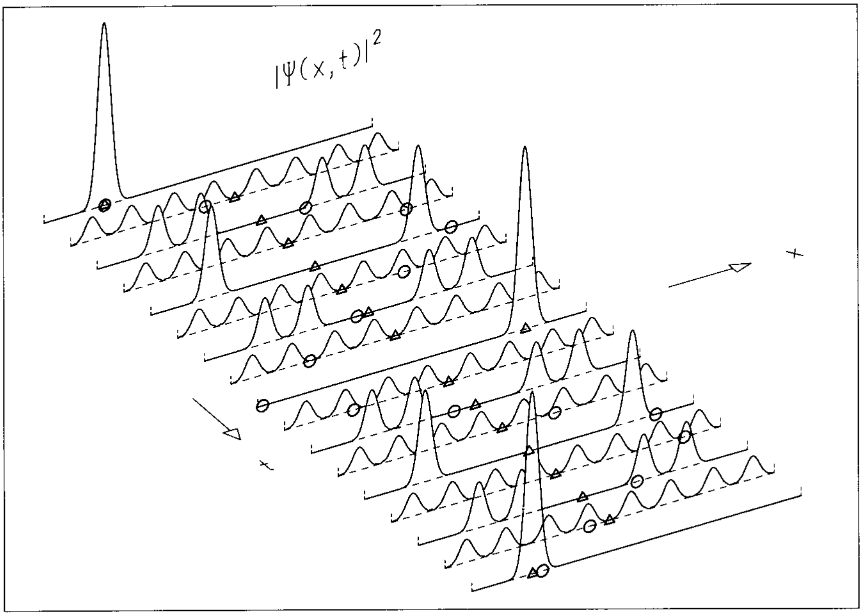

Fig. 6.3. Time development of the same wave packet as in Figure 6.2 but observed of a full revival period T_1. The time interval shown in Figure 6.2 is $T_1/60$.

The periodicity is called *revival* of the wave packet. As we shall see in Section 13.5, the phenomenon is also encountered in the wave-packet motion in the Coulomb potential, e.g., in the hydrogen atom as an approximate revival. To a larger or lesser degree it exists in all systems with discrete spectra of reasonable spacing. In the case of the deep square well it is, however, an exact revival.

In addition to the revival at $t = T_1$ we can also observe *fractional revivals* at the times $t = (k/\ell)T_1$. Here k and ℓ are integer numbers. Since in Figure 6.3 the time T_1 is divided into 16 equal intervals it is easy to observe the packet at the times $t = T_1/2$, $T_1/4$, $T_1/8$, and $T_1/16$. For these times the function $|\psi(x,t)|^2$ consists of 1, 2, 4, and 8 well-separated "Gaussian" humps.

6.3 Spectrum of the Harmonic-Oscillator Potential

The particle in a deep square well experiences a force only when hitting the wall. A simple, continuously acting force $F(x)$ can be thought of as the force of a spring, which follows Hooke's law,

$$F(x) = -kx \quad , \qquad k > 0 \quad .$$

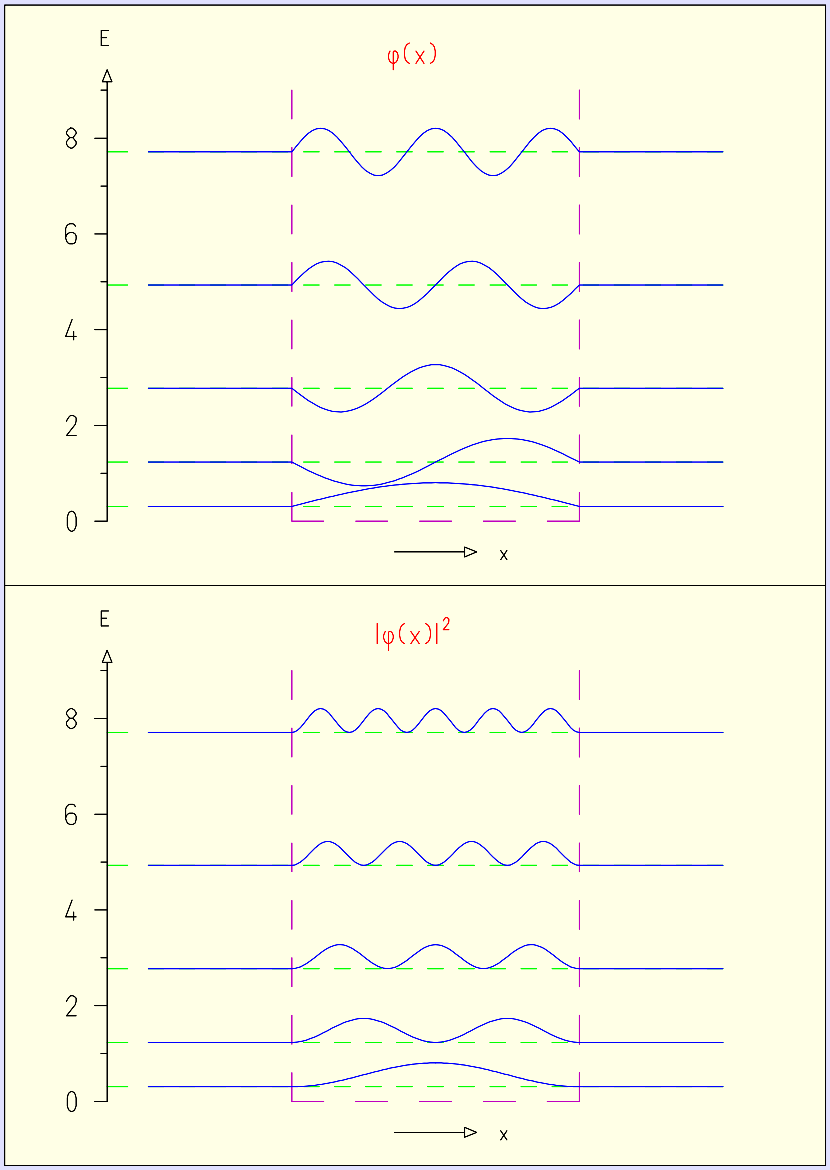

Fig. 6.1. Bound states in an infinitely deep square well. The long-dash line indicates the potential energy $V(x)$. It vanishes for $-d/2 < x < d/2$ and is infinite elsewhere. Points $x = \pm d/2$ are indicated as vertical walls. On the left side an energy scale is drawn, and to the right of it the energies E_n of the lower-lying bound states are indicated by horizontal lines. These lines are repeated as short-dash lines on the left. They serve as zero lines for the wave functions $\varphi(x)$ and the probability densities $|\varphi(x)|^2$ of the bound states.

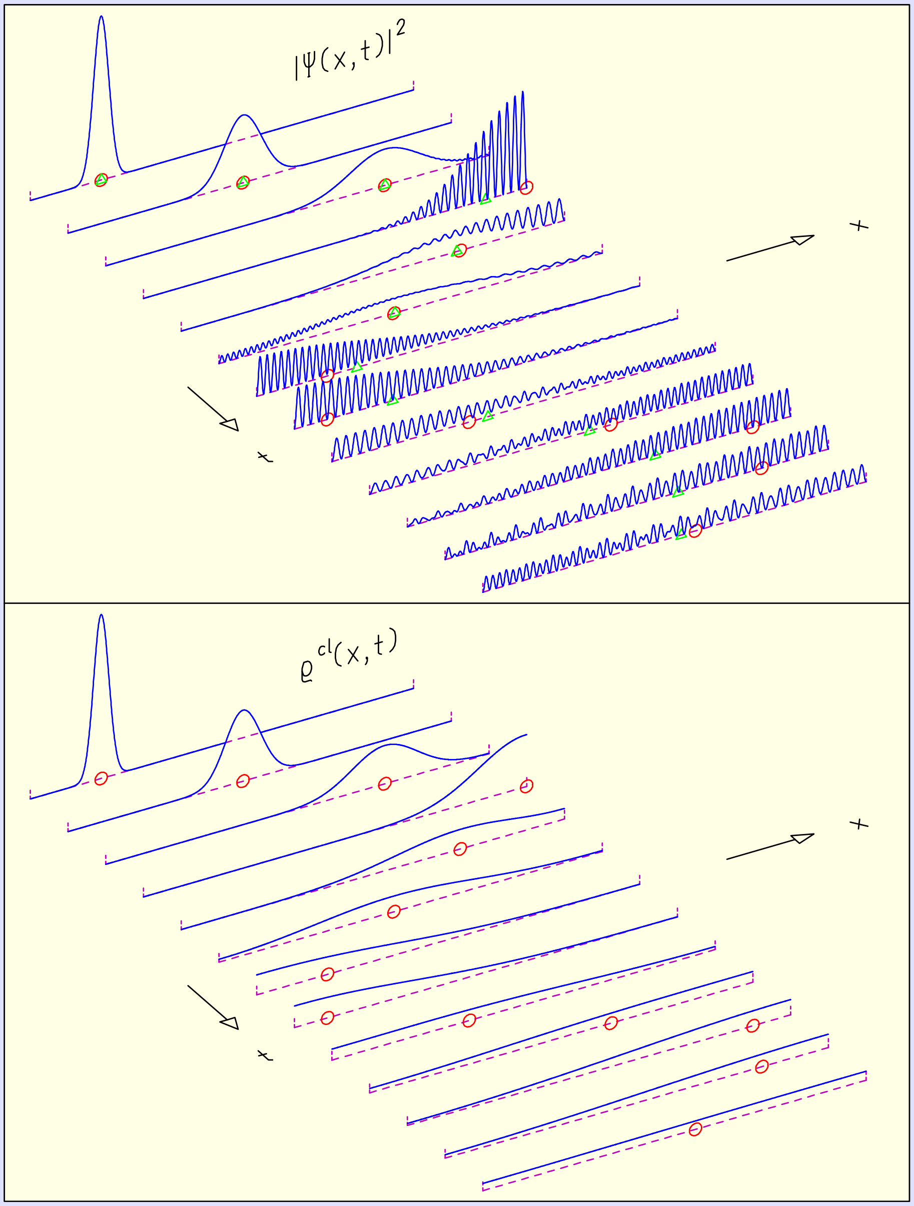

Fig. 6.2. Top: Time development of a wave packet moving in an infinitely deep square well. At $t = 0$, in the background, the smooth packet is well concentrated. Its initial momentum makes it bounce back and forth between the two walls. The characteristic interference pattern of the reflection process, as well as the dispersion of the packet with time, is apparent. The small circle indicates the position of the corresponding classical particle. The quantum-mechanical position expectation value is shown by a small triangle. Bottom: Time development of the spatial probability density computed from the classical phase-space distribution corresponding to the quantum-mechanical wave packet.

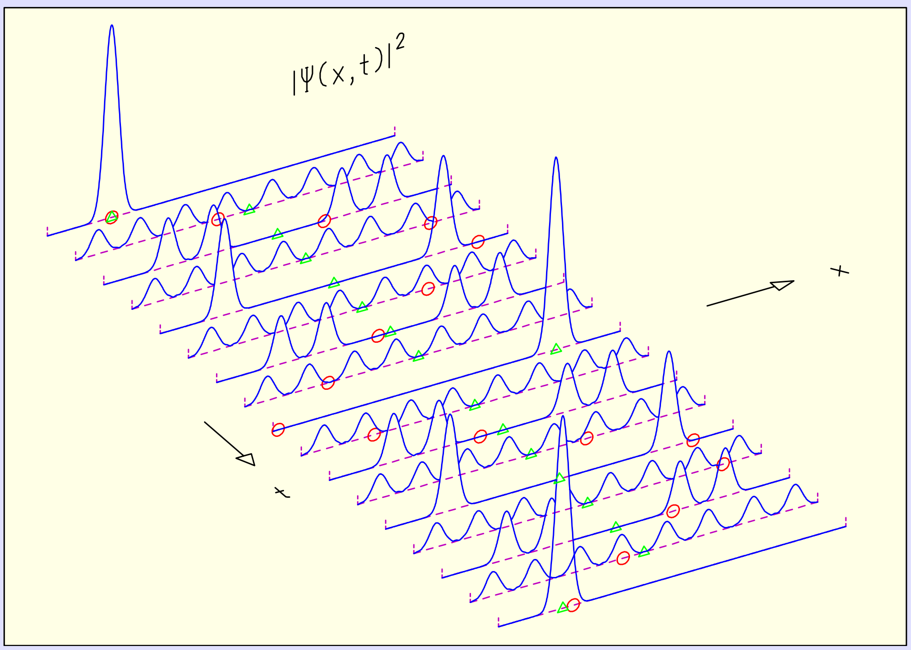

Fig. 6.3. Time development of the same wave packet as in Figure 6.2 but observed of a full revival period T_1. The time interval shown in Figure 6.2 is $T_1/60$.

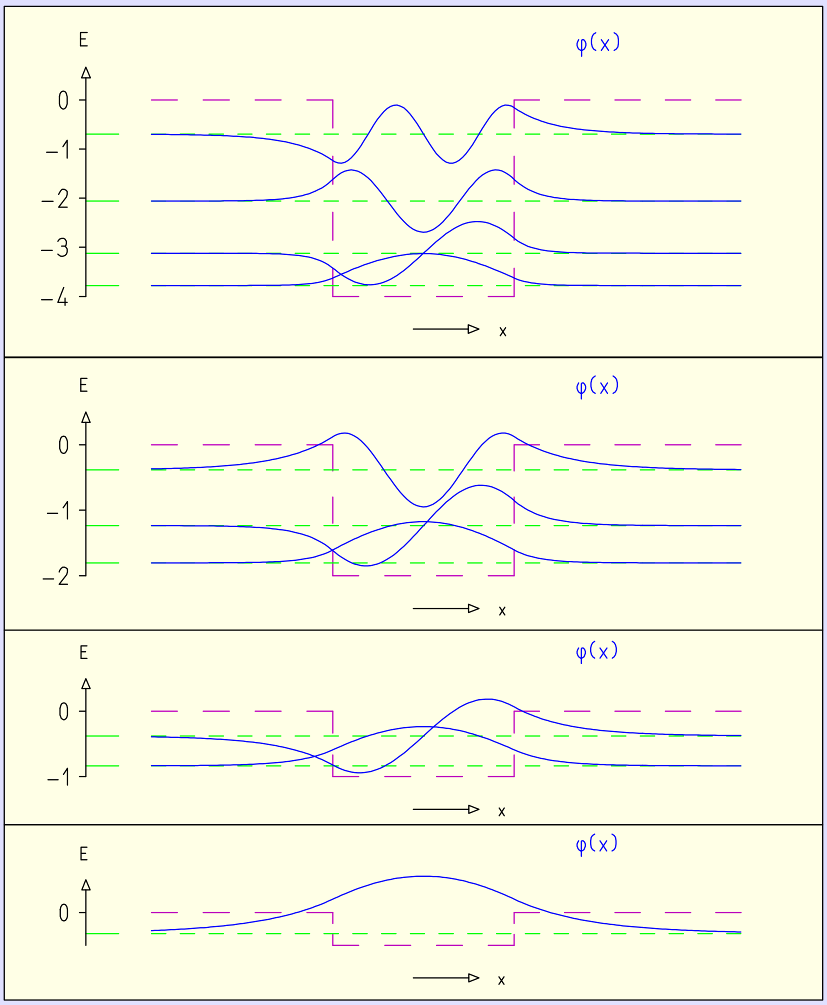

Fig. 6.10. Bound-state wave functions and energy spectra for square-well potentials of different finite depths but identical widths. The number of bound states increases with the depth of the potential.

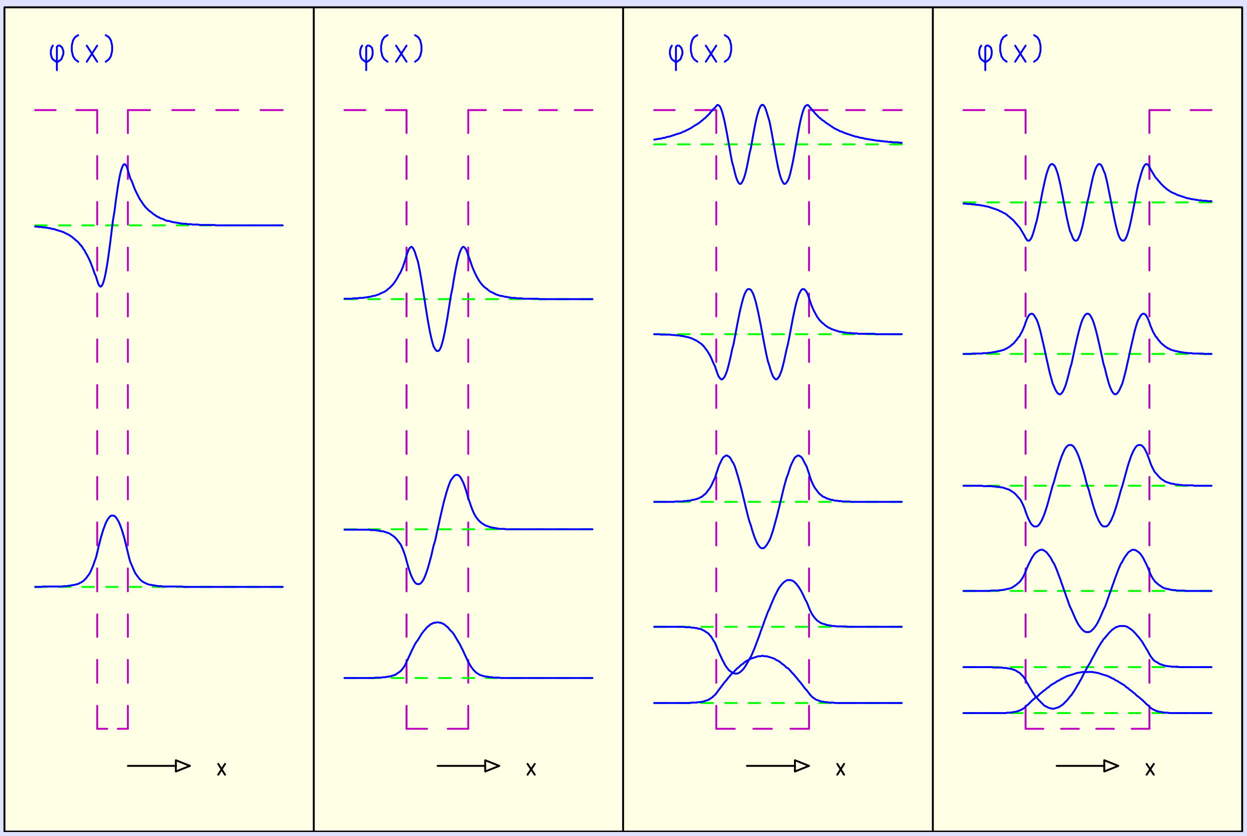

Fig. 6.11. Bound-state wave functions for square-well potentials of identical depth but different widths. The number of bound states increases with the width of the well.

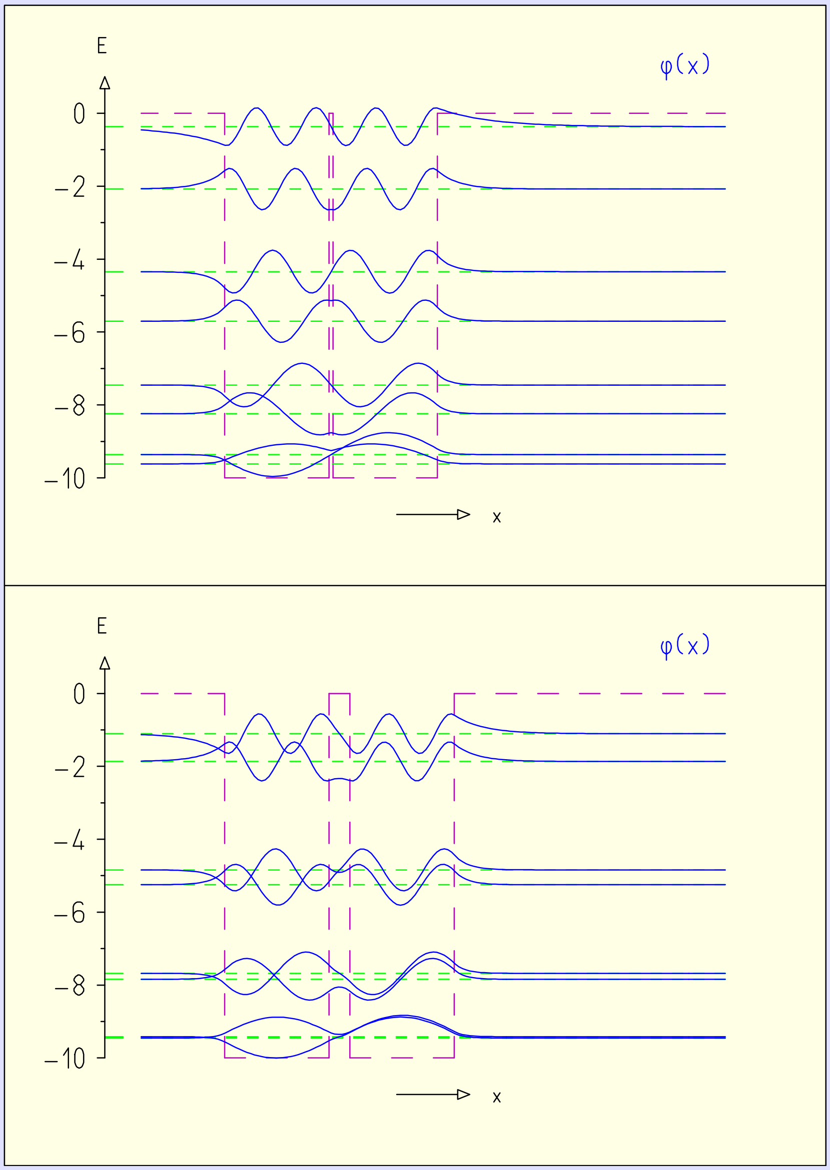

Fig. 6.12. Bound-state wave functions and energy spectra for systems of two square wells. In one system the wells are very close together, in the other some distance apart.

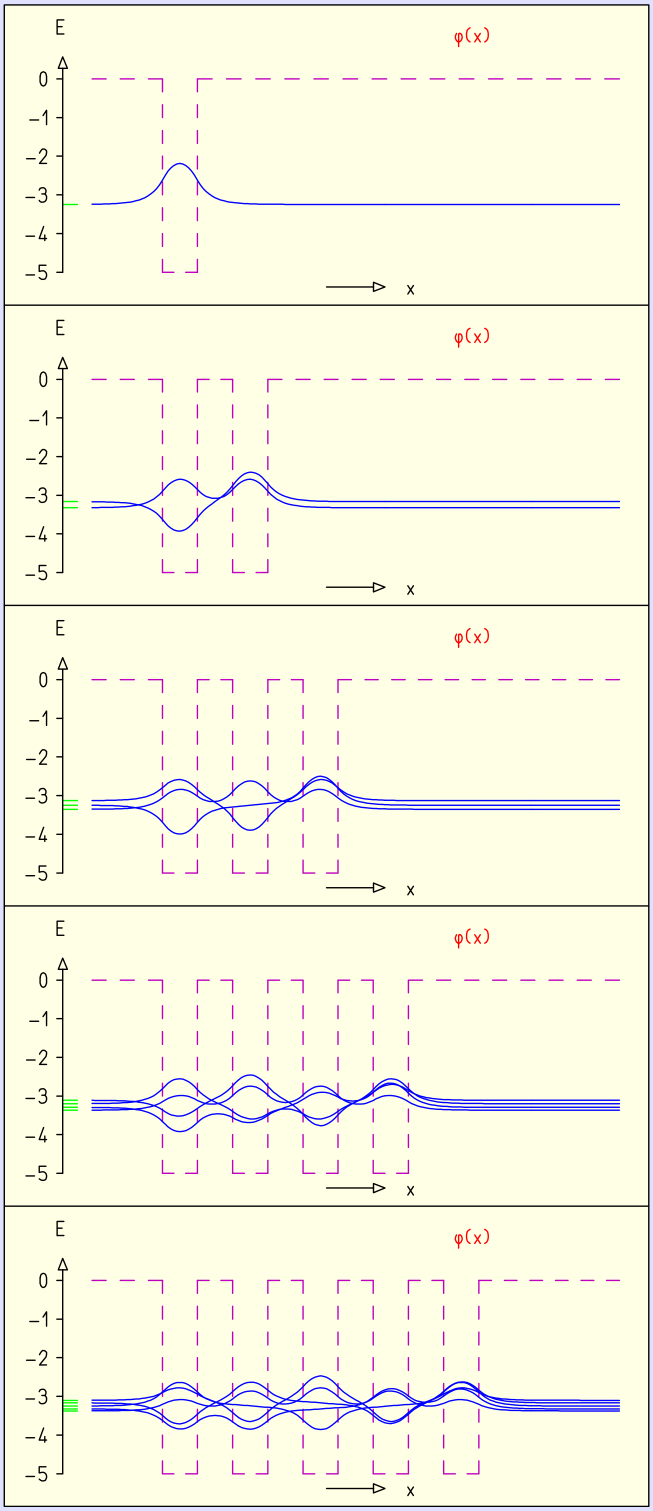

Fig. 6.13. Bound-state wave functions and energy spectra for a potential well and for potentials consisting of two, three, four, and five neighboring wells. The states have very similar energies.